International Journal of Biological Macromolecules 241 (2023) 124386

Contents lists available at ScienceDirect

International Journal of Biological Macromolecules

journal homepage: www.elsevier.com/locate/ijbiomac

Structural characterization and anti-inflammatory activity of polysaccharides from *Astragalus membranaceus*

Guangming Chen [a], Nan Jiang [b,c], Junping Zheng [a], Haiming Hu [a], Huabing Yang [a], Aizhen Lin [b,c], Baifei Hu [a,*], Hongtao Liu [a,*]

[a] College of Basic Medical Sciences, Hubei University of Chinese Medicine, Huangjiahu West Road 16, Wuhan 430065, PR China
[b] Hubei Provincial Hospital of Traditional Chinese Medicine, Wuhan 430061, PR China
[c] Hubei Province Academy of Traditional Chinese Medicine, Wuhan 430074, PR China

ARTICLE INFO

Keywords:
Astragalus membranaceus polysaccharides
Structural characterization
Anti-inflammatory activity

ABSTRACT

In this study, two homogeneous polysaccharides (APS-A1 and APS-B1) were isolated from *Astragalus membranaceus* by DEAE-52 cellulose and Sephadex G-100 column chromatography. Their chemical structures were characterized by molecular weight distribution, monosaccharide composition, infrared spectrum, methylation analysis, and NMR. The results revealed that APS-A1 (2.62×10^6 Da) was a 1,4-α-D-Glc*p* backbone with a 1,4,6-α-D-Glc*p* branch every ten residues. APS-B1 (4.95×10^6 Da) was a heteropolysaccharide composed of glucose, galactose, and arabinose (75.24:17.27:19.35). Its backbone consisted of 1,4-α-D-Glc*p*, 1,4,6-α-D-Glc*p*, 1,5-α-L-Ara*f* and the sidechains composed of 1,6-α-D-Gal*p* and T-α/β-Glc*p*. Bioactivity assays showed that APS-A1 and APS-B1 had potential anti-inflammatory activity. They could inhibit the production of inflammatory factors (TNF-α, IL-6, and MCP-1) in LPS-stimulated RAW264.7 macrophages *via* NF-κB and MAPK (ERK, JNK) pathways. These results suggested that the two polysaccharides could be potential anti-inflammatory supplements.

1. Introduction

Inflammation is a typical defensive response to infection, tissue damage, or harmful stimuli. However, excessive inflammation leads to the occurrence and development of chronic diseases [1]. Many diseases are closely related to excessive inflammatory responses, such as atherosclerosis, liver cirrhosis, diabetes, and cancer [2,3]. Although numerous anti-inflammatory medicines, such as aspirin and corticosteroids, are available to inhibit inflammatory symptoms, long-term usage can result in substantial adverse effects [4]. Studies show that compounds of natural origin have the unique biological activity to intervene in inflammatory diseases, such as polyphenols, flavonoids, and polysaccharides [5,6]. Notably, polysaccharides exhibit good performance in protecting cells from inflammatory cytokine attacks [6]. Thus, they have been considered anti-inflammatory candidates worthy of further study.

Polysaccharides are a kind of natural macromolecular polymer, comprising more than ten monosaccharides linked by glycosidic bonds in linear or branched chains. It is widely distributed in nature and has attracted extensive attention due to various biological activities [7]. For example, four polysaccharides from *Z. jujuba cv. Hamidazao* had significant antioxidant properties *in vitro* [8]. A water-soluble polysaccharide from *Radix Astragali* showed excellent immunomodulatory effects [9]. The bioactivities of polysaccharides are directly associated with their structure, like molecular weight, monosaccharide composition, type of glycosidic bonds, and three-dimensional conformation [10].

Astragalus membranaceus is the dried root of *Astragalus membranaceus* (Fisch.) Bge. or *Astragalus membranaceus* (Fisch.) Bge. Var. *mongholicus* (Bge.) Hsiao. It grows mainly in northern China, Mongolia, and Korea. *A. membranaceus* is a tonic traditional Chinese medicine first recorded in *Shennong's Classic of Materia Medica* [11]. *A. membranaceus* was shown to have many pharmacological activities, such as enhancing immune function, regulating blood glucose and pressure, anti-inflammation, and anti-virus [12–16]. >100 compounds have been isolated from *A. membranaceus*, including saponins, flavonoids, and polysaccharides [17]. Among them, polysaccharides are one of the main active components. Due to low toxicity and unique activity, *A. membranaceus* polysaccharides (APS) have been widely used in the fields of functional foods and medicine [18].

Identification of polysaccharides structure will lay a foundation for

* Corresponding authors.
E-mail addresses: baifeihu@stmail.hbtcm.edu.cn (B. Hu), hongtaoliu@hbtcm.edu.cn (H. Liu).

https://doi.org/10.1016/j.ijbiomac.2023.124386
Received 3 January 2023; Received in revised form 18 March 2023; Accepted 5 April 2023
Available online 11 April 2023

studying pharmacological activity. In this study, we purified the polysaccharides from *A. membranaceus* using DEAE-52 and Sephadex G-100 column chromatography and obtained two homogeneous polysaccharides. And their structures were characterized. Further, based on the LPS-induced RAW264.7 macrophages, we evaluated the anti-inflammatory effects and pharmacodynamic mechanisms of homogeneous APS. Our results will help establish the structure-function relationships of APS and facilitate the application of APS in functional foods and medicines.

2. Materials and methods

2.1. Materials and reagents

Decoction pieces of *A. membranaceus* were provided by Affiliated Hospital of Hubei University of Chinese Medicine. DEAE-52 cellulose was purchased from Shanghai Yuanye Biotechnology Co., Ltd. (Shanghai, China). Sephadex G-100 was obtained from GE Healthcare Biosciences (Pittsburgh, PA, USA). D-glucose was provided by Solarbio Science & Technology Co., Ltd. (Beijing, China). D-galactose and LPS (from *E. coli* 055: B5) were purchased from Sigma (St. Louis, MO, USA). D-arabinose, L-rhamnose, L-fucose, D-mannose, D-galacturonic acid, D-glucuronic acid, and dextran standards with different molecular weight were purchased from Aladdin Co., Ltd. (Shanghai, China). Fetal bovine serum (FBS) was obtained from Gibco (Grand Island, NY, USA), and RPMI 1640 medium was from Corning Incorporated (Corning, NY, USA). Antibodies against P65, p-P65, jun-amino-terminal kinase (JNK), p-JNK, Nod-like receptor protein 3 (NLRP3), inducible nitric oxide synthase (iNOS), cyclooxygenase-2 (COX-2), Inhibitor kappa B alpha (IκB α), IκB kinase-β (IKK-β), p-IKK-α/β, and Histone H3 were purchased from Cell Signaling Technology (Danvers, MA, USA). Antibodies against ERK, p-ERK, p38, p-p38, and β-actin were obtained from Santa Cruz Biotechnology (Santa Cruz, CA, USA).

2.2. Extraction, isolation, and purification of APS

Water-soluble APS was extracted with hot water. The decoction pieces of *A. membranaceus* were dried at 55 °C and crushed into powder (270 μm, 50 mesh screen), then soaked in 90 % ethanol for 24 h to remove lipids. The filter residue was dried at 40 °C and extracted twice with deionized water at 80 °C for 2 h in a ratio of 1:30. The concentrated supernatant was precipitated with four volumes of ethanol at 4 °C overnight. The precipitate was redissolved with deionized water, then deproteinated by Sevag reagent (4:1, *v*/v) (chloroform:n-butanol = 4:1) six times [19]. Next, the solution was mixed with four volumes of ethanol at 4 °C overnight. The precipitate was redissolved and dialyzed (molecular weight cut-off 3500 Da), and freeze-dried to obtain the crude *A. membranaceus* polysaccharide, designated APS.

The APS was redissolved with distilled water, filtered, and purified by anion exchange chromatography. The sample was loaded on a DEAE-52 cellulose column (3.6 × 20 cm) and followed by an elution step with distilled water and different concentrations of NaCl solution (0.1, 0.3, 0.5 mol/L) at a flow rate of 5 mL/min. The eluate (10 mL/tube) was collected and detected by the phenol-sulfuric acid method with glucose as the standard. Four eluent fractions were identified: APS-A, APS-B, APS-C, and APS-D. APS-A and APS-B were two main purified fractions, and their eluent was concentrated, dialyzed (molecular weight cut-off 3500 Da), and lyophilized.

APS-A and APS-B were further purified by Sephadex G-100 column (2.5 × 80 cm), which were eluted with distilled water at a flow rate of 1.0 mL/min. And the eluate (5 mL/tube) was collected and assayed by the phenol-sulfuric acid method. The main purified fractions were dialyzed (molecular weight cut-off 3500 Da), concentrated, and lyophilized to obtain two polysaccharides, *i.e.*, APS-A1 and APS-B1.

2.3. Chemical composition analysis

The total carbohydrate content of APS, APS-A1, and APS-B1 was tested by the phenol-sulfuric acid method, with glucose as the standard [20]. Reducing sugar content was determined by DNS method with D-glucose as the standard [21]. The protein content was evaluated by Bradford method with bovine serum albumin as the standard [22]. The total uronic acid content was measured by *m*-hydroxydiphenyl method with D-glucuronic acid as the standard [23].

2.4. Structure characterization of APS-A1 and APS-B1

2.4.1. Determination of homogeneity and molecular weight

The homogeneity and molecular weight of APS, APS-A1, and APS-B1 were determined by high-performance gel permeation chromatography (HPGPC). The analysis was performed on a Waters high-performance liquid chromatography (HPLC) equipped with a TSK gel GMPWXL column (7.8 mm × 300 mm, 13 μm, TOSOH Co, Tokyo, Japan) and a Waters-2424 evaporative light scattering detector (ELSD). The sample (2.0 mg/mL) was loaded with distilled water as the mobile phase at a flow rate of 0.6 mL/min at 35 °C. The relative molecular weight of polysaccharides was calculated by the standard curve, which was calibrated with dextran standards (Mw: 5, 25, 40, 60, 150, 500, 2000 kDa).

2.4.2. Monosaccharide composition analysis

As stated in our prior publication, the monosaccharide composition was determined by HPLC [24]. Briefly, APS-A1 and APS-B1 were hydrolyzed with trifluoroacetic acid (2 mol/L). The hydrolyzed products were derivatized by 1-phenyl-3-methyl-5-pyrazolone (PMP) and analyzed by HPLC. The standards of the nine monosaccharides were also derivatized according to the same method. The derivatized products were analyzed by Uranus 5u C18 (4.6 mm × 250 mm, 5 μm, FLM Scientific Instrument Co. Ltd., Guangzhou, China).

2.4.3. FT-IR and UV–vis analysis

APS-A1 and APS-B1 were mixed with KBr separately and pressed into pellets, FT-IR spectra were collected on a Nicolet iS50R spectrometer (Thermo Electron Scientific Instruments LLC, WI, USA) over the range 4000–400 cm^{-1}.

APS-A1 and APS-B1 were dissolved in distilled water (2 mg/mL), and the UV spectra of APS-A1 and APS-B1 were recorded in the wavelength range of 200–800 nm by UV–vis spectrophotometer (A590, AOE Instruments, Shanghai, China).

2.4.4. Methylation analysis

Methylation analysis of APS-A1 and APS-B1 was accomplished according to Hakomari method [25]. The polysaccharides were methylated with sodium hydroxide and iodine methane in anhydrous DMSO. The methylation products were analyzed by FT-IR, and the disappearance of the –OH absorption peak indicated that the polysaccharides were completely methylated. The methylation products were hydrolyzed with trifluoroacetic acid, followed by reduction with $NaBH_4$ and acetylation with acetic anhydride. Finally, partially methylated alditol acetates (PMAAs) were analyzed by GC–MS system with a DB-5MS capillary column (30 m × 0.5 cm × 0.25 μm).

2.4.5. NMR spectroscopy analysis

Structural information of APS-A1 and APS-B1 was analyzed by NMR spectroscopy. The APS-A1 (50 mg) or APS-B1 (50 mg) was dissolved in deuterium oxide (D_2O, 0.6 mL, 99.9 %) in an NMR tube and kept at room temperature overnight. The 1D NMR spectra (including ^1H NMR and ^{13}C NMR) and 2D NMR spectra (including HSQC, COSY, and HMBC spectra) of APS-A1 and APS-B1 were recorded on a Bruker AVANCE HD III 600 MHz spectrometer (Bruker, Rheinstetten, Germany) at 298 K.

2.5. Anti-inflammatory activity assay of APS-A1 and APS-B1 in vitro

2.5.1. Cell culture and treatment

RAW264.7 cells, a murine macrophage cell line, were obtained from American Type Culture Collection (ATCC, Manassas, VA, USA). Cells were cultured in RPMI-1640 medium supplemented with 10 % heat-inactivated FBS, penicillin (100 U/ mL), and streptomycin (100 μg/ mL) at 37 °C in a 5 % CO_2 humidified atmosphere. After cell density reached 70 %, cells were treated with LPS (1 μg/mL) or different concentrations of APS-A1 and APS-B1 (0–200 μg/mL) for another 1–24 h. Then, cells were collected for subsequent experiments.

2.5.2. Cell viability assay

Cell viability was evaluated by methyl thiazolyl tetrazolium (MTT) reduction colorimetric assay. RAW264.7 cells were seeded in 96-well plates. Then, APS-A1 or APS-B1 were added at different concentrations (0, 12.5, 25, 50, 100, and 200 μg/mL). After cells were incubated for 24 h, MTT (0.2 mg/mL) was added into each well and kept for 4 h. Afterwards, the supernatants were removed, and 100 μL of dimethyl sulfoxide (DMSO) was used to solubilize the formazan crystals. The absorbance was measured at 490 nm with a microplate reader (Molecular Devices Corporation, San Jose, CA, USA). Cell survival was expressed as a percentage, and the experiment was repeated three times.

2.5.3. RNA extraction and real-time quantitative PCR (RT-PCR)

Total RNA was extracted from the collected cells using Trizol reagent (Summer Bio, Beijing, China). The isolated RNA was reverse transcribed into cDNA by first strand cDNA synthesis kit (Summer Bio, Beijing, China). RT-PCR was performed on a BIO-RAD CFX Connect real-time fluorescence quantification system (BioRad, CA, USA) with the following reaction parameters: 95 °C for 10 min; 45 cycles of amplification (95 °C for 10 s, 60 °C for 30 s). The target gene primer sequences were shown in Supplementary Table 1, including interleukin-1β (IL-1β), interleukin-6 (IL-6), tumor necrosis factor-α (TNF-α), monocyte chemotactic protein-1 (MCP-1), and β-actin. All mRNA levels were normalized using β-actin as an internal reference, and the relative expression of genes was calculated by the $2^{(-\Delta\Delta Ct)}$ method.

2.5.4. Cytokine measurement

RAW264.7 cells were seeded in 24-well plates, pretreated with APS-A1 or APS-B1 for 12 h, and then treated with LPS (1 μg/mL) for 24 h. The supernatants were collected and centrifuged at 1000 ×*g* for 20 min to remove cell debris. The levels of IL-6, TNF-α, and MCP-1 in supernatants were analyzed by sandwich enzyme-linked immunosorbent assay (ELISA) with commercially available ELISA kits (Elabscience Biotechnology, Wuhan, China) according to the manufacturer's instructions.

2.5.5. Western blot analysis

The protein extraction and immunoblot analysis were performed using the methods described in the previous report [26]. Briefly, the cells were collected, washed in PBS, and lysed in IP lysis buffer (Beyotime Biotechnology, Shanghai, China) supplemented with protease inhibitor mixture (Merck, Darmstadt, Germany) to extract total proteins. Proteins from the nuclear and cytoplasmic fractions of cells were extracted using Nuclear and Cytoplasmic Protein Extraction Kit (Beyotime Biotechnology, Shanghai, China) according to the manufacturer's instructions. After quantification of protein concentrations using the BCA protein assay kit (Beyotime Biotechnology, Shanghai, China), protein samples were separated by SDS-polyacrylamide gel electrophoresis and transferred onto PVDF membranes (Millipore, Bedford, MA, USA). After blocking the non-specific sites with 5 % nonfat milk, the membranes were treated overnight at 4 °C with primary antibodies. The membranes were then treated for 1 h at room temperature with horseradish peroxidase-coupled secondary antibodies. The protein bands were seen with an enhanced chemiluminescence kit (Summerbio, Beijing, China), and densitometry was performed with Image J2x software (National Institute of Health, Bethesda, MD, USA).

2.5.6. Immunofluorescence

RAW264.7 cells cultured on sterile coverslips were pretreated with APS-A1 or APS-B1 for 12 h before being stimulated with LPS (1 μg/mL) for 1 h. The cells were then fixed in 4 % paraformaldehyde for 20 min. Coverslips were incubated with primary antibody (1:100) at 4 °C in PBS containing 1 % BSA and 0.05 % Triton X-100. After washing, cells were incubated with a secondary antibody coupled with Dylight 488 at room temperature for 1 h, and nuclei were labeled with 4′, 6-diamidino-2-phenylindole (DAPI). Immunofluorescence images were collected and analyzed using Nikon Intensilight C-HGFI microscope (Nikon, Melville, NY, USA).

2.6. Statistical analysis

All statistical analysis were performed by GraphPad Prism 8.0. All data are expressed as mean ± standard deviation (SD). All experiments were performed at least three times. Data were analyzed by one-way analysis of variance (ANOVA) and Duncan's multiple range test for comparison between multiple groups. Values of $p < 0.05$ were considered statistically significant.

3. Results

3.1. Extraction, isolation, and purification of polysaccharides

The procedure to extract and purify polysaccharides from *A. membranaceus* was schematically depicted in Fig. 1A. The crude polysaccharides (APS) with a yield of 8.80 % were first separated by DEAE-52 cellulose column chromatography. Four elution peaks were obtained, named APS-A, APS-B, APS-C, and APS-D (Fig. 1B), and the yields of each fraction were 11.74 %, 15.28 %, 4.13 %, and 3.91 %, respectively. Among them, APS-A and APS-B were further purified using Sephadex G-100 gel column. As shown in Fig. 1C and D, two elution peaks were obtained from APS-A and APS-B, denominated APS-A1 and APS-B1, with yields of 46.10 % and 86.84 %, respectively.

3.2. Chemical composition analysis

The contents of chemical components of crude and purified polysaccharides were analyzed. The contents of total carbohydrates, proteins, reducing sugars, and uronic acid of APS, APS-A1, and APS-B1 were listed in Table 1. The total carbohydrate content of APS was 64.03 %, and the protein content was 9.04 %. After purification, the total carbohydrate content of APS-A1 reached 99.48 %, which was a neutral polysaccharide. The total carbohydrate content of APS-B1 was 97.51 %, and the uronic acid content was 1.16 %, indicating that APS-B1 was a weakly acidic polysaccharide. Meanwhile, no protein and reducing sugar were detected in APS-A1 and APS-B1.

3.3. Structural analysis of APS-A1 and APS-B1

3.3.1. Homogeneity and molecular weight

Next, we determined the homogeneity and average molecular weight of APS-A1 and APS-B1 by HPGPC. As shown in Fig. 2A, the molecular weight distribution of APS was wide and heterogeneous. After purification, the HPGPC profiles of APS-A1 and APS-B1 exhibited single symmetrical peaks. The retention times of APS-A1 and APS-B1 were 9.78 min and 9.25 min, respectively. Based on the regression equation of the dextran standard curve log $M_W = 11.51–0.5206$ t (t means retention time, $R^2 = 0.9947$), the mean molecular weight of APS-A1 and APS-B1 were calculated as 2.62×10^6 Da and 4.95×10^6 Da.

3.3.2. Monosaccharide composition analysis

Monosaccharide composition analysis were indicated in Table 1 and

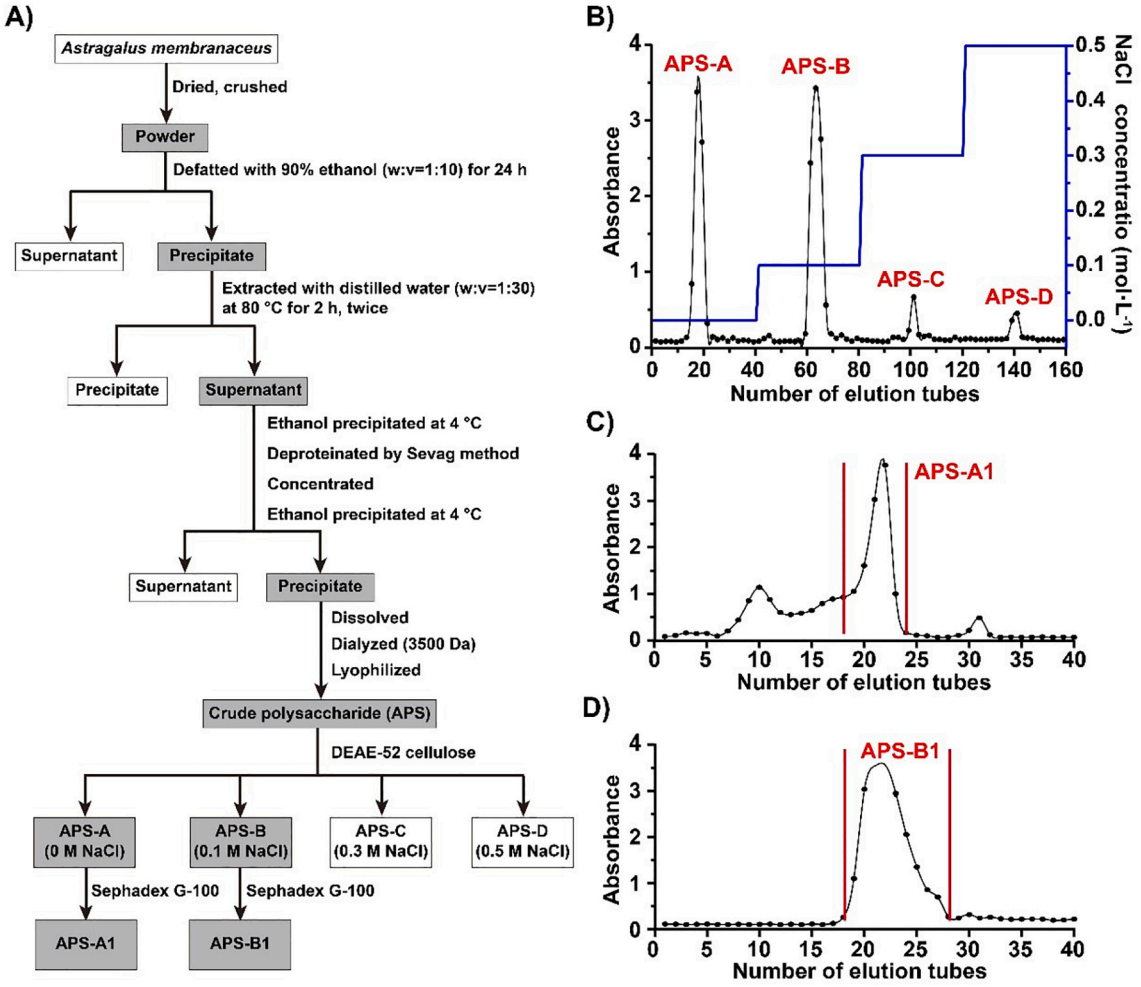

Fig. 1. Extraction and purification of APS. (A) Preparation flow diagram of APS. (B) Elution curve of APS on DEAE-52 cellulose column. (C-D) Elution curve of APS-A (C) and APS-B (D) on Sephadex G-100 column.

Table 1
Chemical composition for APS-A1 and APS-B1.

Samples	APS	APS-A1	APS-B1
Chemical compositions			
Total carbohydrate (%)	64.03 ± 0.43	99.48 ± 1.30	97.51 ± 0.85
Protein (%)	9.04 ± 0.24	ND	ND
Reducing sugar (%)	3.34 ± 0.02	ND	ND
Uronic acid content (%)	3.30 ± 0.10	ND	1.16 ± 0.02
Monosaccharide composition (molar ratio, %)			
Glucose		95.76	65.26
Galactose		1.83	14.98
Arabinose		2.41	16.79
Mannose		ND	0.87
Rhamnose		ND	0.94
Galacturonic acid		ND	1.16

ND: Not detected or lower than limit of quantification.

Fig. 2B. APS-A1 was composed of glucose, galactose, and arabinose in a molar ratio of 52.3:1.0:1.3. APS-B1 consisted of glucose, galactose, arabinose, mannose, rhamnose, and galacturonic acid in a molar ratio of 75.2:17.3:19.4:1.0:1.1:1.3. APS-A1 was a neutral polysaccharide, and APS-B1 was a weakly acidic heteropolysaccharide, which was consistent with the results of chemical composition.

3.3.3. UV–vis and FT-IR spectra

FT-IR spectroscopy is an effective method to characterize the functional groups of polysaccharides. The FT-IR spectra of APS-A1 and APS-B1 in the range of 4000–400 cm^{-1} were shown in Fig. 2C, which displayed typical characteristic absorption peaks of polysaccharides [27]. Specifically, the broad and intense peak at around 3420 cm^{-1} was assigned to the O—H stretching vibration, and the peak at 2929 cm^{-1} was assigned to the C—H stretching band. The absorption band at 1646 cm^{-1} was due to bound water, and the peaks at 1416 cm^{-1} and 1368 cm^{-1} were assigned to C—H bending vibrations [28]. The three characteristic absorption peaks between 1200 and 1000 cm^{-1} were attributed to the stretching vibration of pyranose [29]. In addition, the weak peaks near 850 cm^{-1} confirmed the presence of α-configuration glycosidic bonds [30].

The UV–vis spectra of APS-A1 and APS-B1 were presented in Fig. 2D. No significant absorption peaks were observed at 260 nm and 280 nm, indicating that neither contained nucleic acids or proteins [31]. The results were consistent with the chemical analysis (Table 1).

3.3.4. Methylation analysis

Methylation analysis was conducted to reveal the glycosidic linkages in APS-A1 and APS-B1. The results of methylation analysis were presented in Table 2. Compared to the standard database (The CCRC Spectral Database for PMAA's), three main glycoside linkages were attributed to T-Glc*p*, 1,4-Glc*p*, and 1,4,6-Glc*p* residues with a molar ratio of 1.87:9.93:1.00 (Table 2). Among them, the content of 1,4-Glc*p*

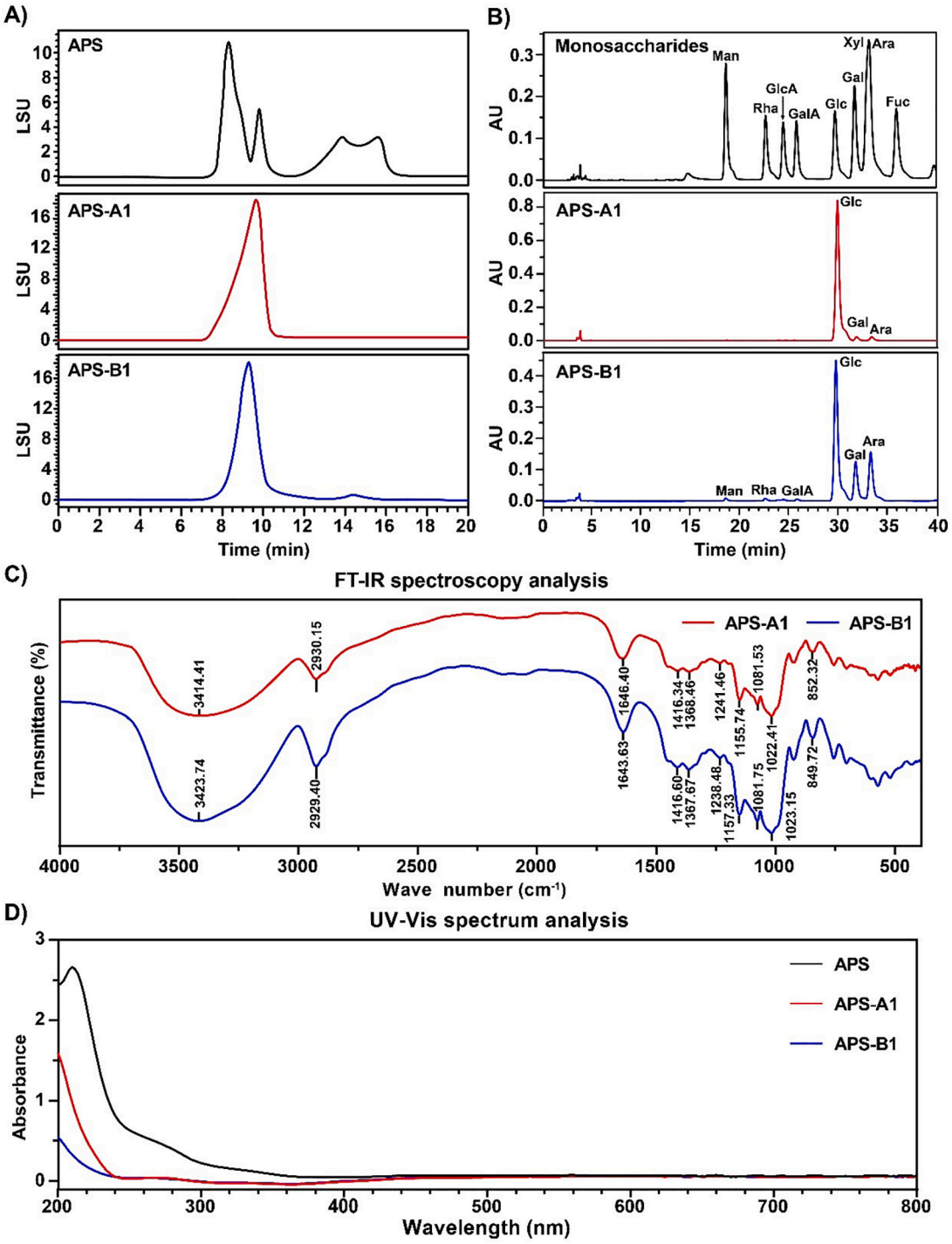

Fig. 2. Physicochemical properties and spectral analysis of APS-A1 and APS-B1. (A) HPGPC chromatograms of APS-A1 and APS-B1. (B) HPLC chromatograms of nine standard monosaccharides and hydrolysis products of APS-A1 and APS-B1. (C) FT-IR spectra of APS-A1 and APS-B1. (D) UV–vis spectra of APS-A1 and APS-B1. Man, mannose. Rha, rhamnose; GlcA, glucuronic acid; GalA, galacturonic acid; Glc, glucose; Gal, galactose; Xyl, xylose; Ara, arabinose; Fuc, fucose.

accounted for 77.58 %, which indicated that the main chain of APS-A1 might be composed of 1,4-Glc*p* repeating units. Signals of galactose and arabinose were not apparent, probably due to their low percentage in APS-A1 (Table 1).

As for APS-B1, methylation analysis revealed that APS-B1 contained five residues, namely 1,5-Ara*f*, T-Glc*p*, 1,4-Glc*p*, 1,6-Gal*p*, and 1,4,6-Glc*p* residues, with molar ratio of 0.24:1.89:11.08:1.03:1.00 (Table 2). These results illustrated that the main chain of APS-B1 consisted of 1,4-Glc*p*, while 1,5-Ara*f* and 1,6-Gal*p* might be present in the branched chains. In addition, the methylation analysis showed a lower proportion of arabinose residues than those detected in the monosaccharide composition analysis (16.79 %), and the undetected arabinose residues might result from losses caused by hydrolysis, reduction, and acetylation during the methylation analysis process [32].

3.3.5. NMR analysis

NMR analysis is currently one of the effective methods for the structural analysis of polysaccharides. Both 1D NMR and 2D NMR spectra of APS-A1 and APS-B1 were used to assign the ^{1}H and ^{13}C chemical shifts for sugar residues, and the results were shown in Table 3.

Table 2
Results of methylation analysis for APS-A1 and APS-B1.

Samples	Retention time (min)	Methylated alditol acetate	Mass fragments (*m/z*)	Type of linkage	Molar ratio
APS-A1	29.99	2, 3, 4, 6-Me_4-Glc	43, 59, 71, 87, 101, 117, 129, 145, 161, 205	D-Glc*p*-(1→	1.87
	35.13	2, 3, 6-Me_3-Glc	43, 59, 71, 87, 99, 101, 113, 117, 129, 142, 159, 173, 233	→4)-α-D-Glc*p*-(1→	9.93
	41.10	2, 3-Me_2-Glc	43, 71, 87, 101, 117, 127, 142, 161, 201, 261	→4, 6)-α-D-Glc*p*-(1→	1.00
APS-B1	22.41	2, 3-Me_2-Ara	43, 59, 71, 87, 101, 117, 129, 141, 161, 189	→5)-α-D-Ara*p*-(1→	0.24
	29.98	2, 3, 4, 6-Me_4-Glc	43, 59, 71, 87, 101, 117, 129, 145, 161, 205	D-Glc*p*-(1→	1.89
	35.13	2, 3, 6-Me_3-Glc	43, 59, 71, 87, 99, 101, 113, 117, 129, 142, 159, 173, 233	→4)-α-D-Glc*p*-(1→	11.08
	35.47	2, 3, 4-Me_3-Gal	43, 59, 71, 87, 99, 101, 113, 117, 129, 161, 189	→6)-α-D-Gal*p*-(1→	1.03
	41.09	2, 3-Me_2-Glc	43, 71, 87, 101, 117, 127, 142, 161, 201, 261	→4, 6)-α-D-Glc*p*-(1→	1.00

For APS-A1, ^{1}H NMR and ^{13}C NMR spectra were given in Fig. 3A and B. According to HSQC spectra, the chemical shifts of anomeric protons/carbons for residues A–D were 99.6/5.33 ppm (A1), 99.7/5.32 ppm (B1), 98.8/4.90 ppm (C1), 96.5/4.56 ppm (D1), respectively (Fig. 3A–3D). The anomeric signals (> 4.9 ppm) of A, B, and C indicated that they were α-configurations, consistent with the presence of FT-IR absorption peak at 852 cm^{-1}. Moreover, a weak intensity anomeric signal was observed at (96.5/4.56) D1, characterized by the β-configuration [33].

The chemical shift signals of other hydrogens and carbons were attributed based on 2D NMR (COSY, HSQC) (Fig. 3C, D) and literature [34] (Table 3), and residue A was tentatively determined to be 1,4-α-D-Glc*p*. Residue B was identified as 1,4,6-α-D-Glc*p*, residue C was assigned as terminal-α-D-Glc*p*, and residue D was identified as terminal-β-D-Glc*p*. The presence of residue D indicated the presence of both α- and β-configuration glucose at the terminus of APS-A1 [35].

Based on the cross peaks seen in the HMBC (Fig. 3E), the linkage sequence among these residues of APS-A1 was determined. The signals at 5.33/76.7 ppm (AH1-AC4) and 3.55/99.6 ppm (AH4-AC1) indicated the presence of →4)-α-D-Glc*p*-(1 → 4)-α-D-Glc*p*-(1 → structures. The signals at 5.32/76.7 ppm (BH1-AC4) and 3.54/99.6 ppm (BH4-AC1) showed that both C-1 and C-4 of 1,4,6-α-D-Glc*p* were linked to 1,4-α-D-Glc*p*.

Based on the above results, it was hypothesized that the backbone of APS-A1 was 1,4-α-D-Glc*p*, with some of the 1,4-α-D-Glc*p* attached to the terminal-α/β-D-Glc*p* at O-6. Therefore, the predicted repeating unit of APS-A1 was proposed, as shown in Fig. 5A and C.

For APS-B1, the anomeric region of the HSQC (Fig. 4D) showed six signals at 5.36/99.6 ppm (A1), 5.34/99.7 ppm (B1), 5.16/100.4 ppm (C1), 5.03/107.4 ppm (D1), 4.90/98.8 ppm (E1), and 4.58/95.7 ppm (F1). According to the 2D NMR spectra (Fig. 4C and D), the chemical shift of other protons and carbon were attributed and summarized in Table 3. Among them, the four residues A, B, E, and F were the same as A, B, C, and D in APS-A1, which were determined as 1,4-α-D-Glc*p*, 1,4,6-α-D-Glc*p*, terminal-α-D-Glc*p*, and terminal-β-D-Glc*p*. In addition, residue C was assigned as 1,6-α-D-Gal*p* [36].

The chemical shift of Ara*f* anomeric carbon is typically close to 110 ppm, and this characteristic signal is easily identified [37], so the signal of D (5.03/107.4) was assigned to α-1,5-L-Ara*f*. The H-2/C-2 was confirmed to be 4.07/81.3 ppm, and the H-3/C-3 was 3.89/73.4 ppm according to HSQC and COSY, suggesting that C-2 and C-3 of D were not involved in glycosidic bond formation. The signal of 4.15/80.7 ppm was attributed to H-4/C-4, and the high chemical shift of C-4 indicated the involvement of C-5 in the formation of glycosidic bonds. Therefore, D was attributed to 1,5-α-L-Ara*f*.

The sequence of the glycosyl residues in APS-B1 was determined based on HMBC spectrum (Fig. 4E). In addition to the same signal as HMBC spectrum of APS-A1, the signals at 5.34/64.8 ppm (BH1-DC5) and 3.77/99.7 ppm (DH5-BC1) showed the presence of →4,6)-α-D-Glc*p*-(1 → 5)-α-L-Ara*f*-(1 → structures. The signal at 5.16/69.8 ppm (CH1-BC6) indicated that the C-6 position of 1,4,6-α-D-Glc*p* is replaced by 1,6-α-D-Gal*p*. The signal at 3.58/107.4 ppm (AH4-DC1) showed that C-1 of 1,5-α-L-Ara*f* was linked to O-4 of 1,4-α-D-Glc*p*. The signal at 4.90/69.4 ppm (EH1-CC6) suggested that the end of 1,6-α-D-Galp was attached to

Table 3
NMR ^{1}H and ^{13}C chemical shift assignments of APS-A1 and APS-B1 (ppm).

Samples	Number	Chemical shifts (δ, ppm)						Residue
		H1/C1	H2/C2	H3/C3	H4/C4	H5/C5	H6/C6	
APS-A1	A	5.33	3.58	3.90	3.55	3.77	3.75	→4)-α-D-Glc*p*-(1→
		99.6	71.7	73.3	76.7	71.5	60.4	
	B	5.32	3.58	3.90	3.54	3.63	3.35	→4, 6)-α-D-Glc*p*-(1→
		99.7	71.7	72.8	76.7	72.7	69.3	
	C	4.90	3.51	3.88	3.65	3.72	3.81	α-D-Glc*p*-(1→
		98.8	71.7	76.7	72.9	71.2	60.7	
	D	4.56	3.19	3.74	3.91	3.57	3.72	β-D-Glc*p*-(1→
		96.5	73.8	76.7	71.3	76.7	60.4	
APS-B1	A	5.36	3.57	3.90	3.58	3.77	3.74	→4)-α-D-Glc*p*-(1→
		99.6	71.8	73.6	76.5	71.5	60.6	
	B	5.34	3.55	3.90	3.58	3.61	3.36	→4, 6)-α-D-Glc*p*-(1→
		99.7	71.8	73.6	76.5	72.5	69.8	
	C	5.16	3.49	3.76	3.93	4.02	3.67	→6)-α-D-Gal*p*-(1→
		100.4	73.1	71.4	70.8	70.4	69.4	
	D	5.03	4.07	3.89	4.15	3.77	–	→5)-α-L-Ara*f*-(1→
		107.4	81.3	73.4	80.7	64.8	–	
	E	4.90	3.53	3.88	3.65	3.68	3.79	α-D-Glc*p*-(1→
		98.8	72.1	76.7	72.9	73.0	60.6	
	F	4.58	3.21	3.69	3.91	3.57	3.75	β-D-Glc*p*-(1→
		95.7	74.0	76.3	70.8	76.7	60.4	

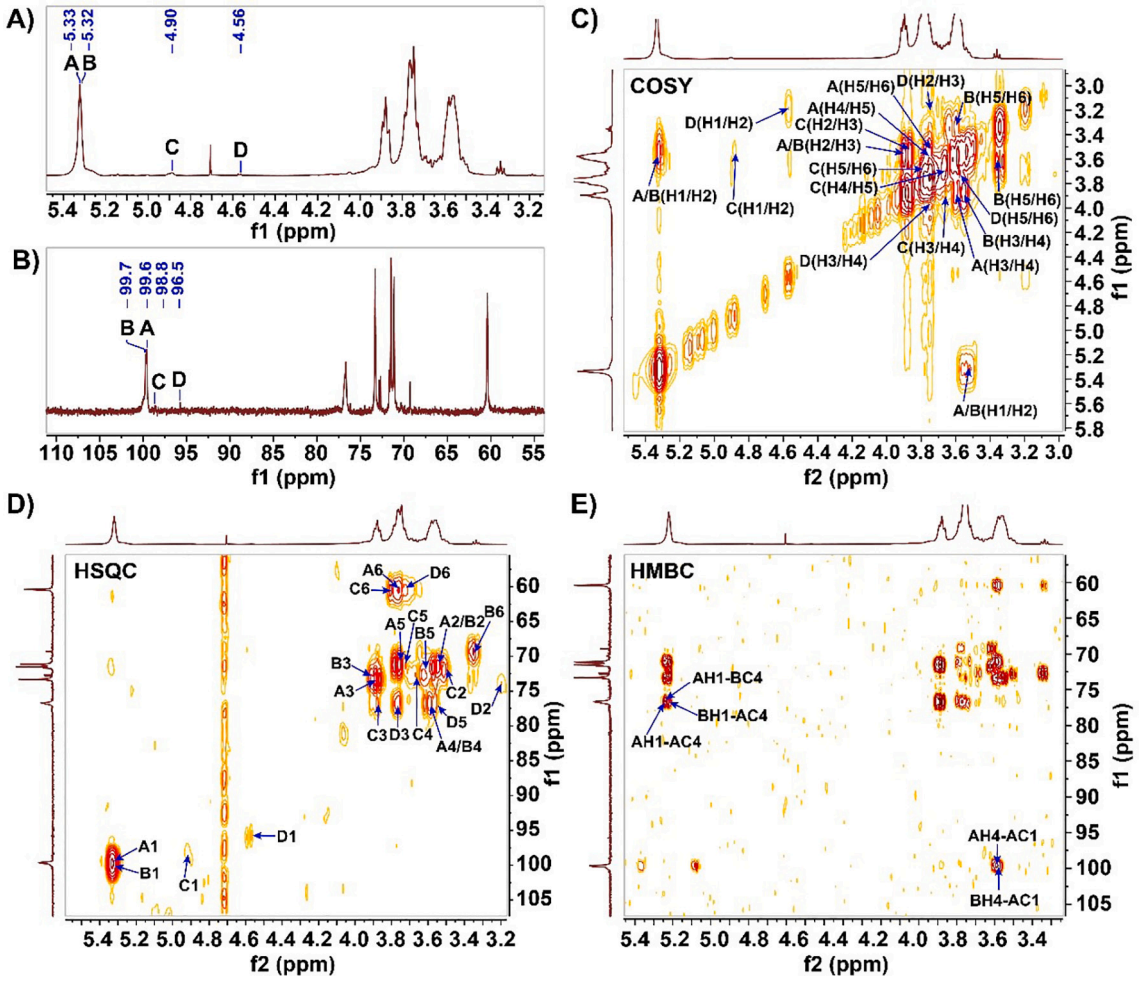

Fig. 3. NMR spectra of APS-A1. (A) ^{1}H NMR spectrum. (B) ^{13}C NMR spectrum. (C) COSY spectrum. (D) HSQC spectrum. (E) HMBC spectrum.

terminal-α/β-D-Glc*p*.

Based on the above results, it was hypothesized that the backbone of APS-B1 was 1,4-α-D-Glc*p* interspersed with 1,5-α-L-Ara*f*, and branches were attached to the backbone at O-6 of some 1,4-α-D-Glc*p*. The branches were supposed to be 1,6-α-D-Gal*p* and terminated by α/β-Glc*p* residues. Therefore, the predicted repeating unit of APS-B1 was proposed, as shown in Fig. 5B and D. Furthermore, the percentage of other monosaccharides (Man*p*, Rha*p*, Gal*p*A) in APS-B1 is relatively limited, so the NMR signal of the anomeric signal is too weak to be detected.

3.4. Anti-inflammatory activity of APS-A1 and APS-B1

3.4.1. Effect of APS-A1 and APS-B1 on viability of RAW264.7 macrophages

The effect of APS-A1 and APS-B1 on the viability of RAW264.7 cells was determined by MTT assay. RAW264.7 cells were incubated with different concentrations (12.5, 25, 50, 100, and 200 μg/mL) of APS-A1 or APS-B1 for 24 h. The results showed no significant change in cell viability, indicating that both polysaccharides had no toxicity to RAW264.7 cells within 200 μg/mL (Fig. 6A and B).

3.4.2. APS-A1 and APS-B1 suppressed LPS-induced inflammation in RAW264.7 macrophages

To determine the effect of APS-A1 and APS-B1 on the inflammatory response, we detected the expressions of LPS-induced proinflammatory cytokines in RAW264.7 macrophages at the mRNA level. As shown in Fig. 6C–F, the expression levels of TNF-α, IL-1β, IL-6, and MCP-1 were significantly increased in the LPS group ($p < 0.01$, *vs.* Control group). And APS-A1 and APS-B1 treatment (50, 100, and 200 μg/mL) markedly inhibited the up-regulation of the above-mentioned inflammatory factors in a concentration-dependent manner ($p < 0.01$, *vs.* LPS group) (Fig. 6C–F). In addition, the results of ELISA showed that both APS-A1 (200 μg/mL) and APS-B1 (200 μg/mL) dramatically suppressed the production of IL-6, TNF-α, and MCP-1 ($p < 0.01$, *vs.* LPS group) (Fig. 6G–I).

3.4.3. APS-A1 and APS-B1 down-regulated expressions of NLRP3, iNOS, and COX-2 in LPS-induced RAW264.7 macrophages

NLRP3, iNOS, and COX-2 are significant pro-inflammatory mediators that play a critical role in developing oxidative stress and inflammation [38]. As shown in Fig. 7A–C, the protein levels of NLRP3, iNOS, and COX-2 were significantly increased by LPS stimulation. And the intervention of APS-A1 (200 μg/mL) and APS-B1 (200 μg/mL) reversed the above abnormal protein changes ($p < 0.05$ or 0.01, *vs.* LPS group) (Fig. 7A–C).

3.4.4. APS-A1 and APS-B1 attenuated phosphorylation of MAPK in LPS-induced RAW264.7 macrophages

To further explore the mechanism of APS-A1 and APS-B1 inhibiting inflammation, we investigated their effects on two important signaling pathways in the inflammatory response, namely the nuclear transcription factor kappa-B (NF-κB) signaling pathway and mitogen-activated protein kinases (MAPK) signaling pathway [39]. First, we detected the phosphorylation of JNK, ERK, and p38 by western blot analysis. The

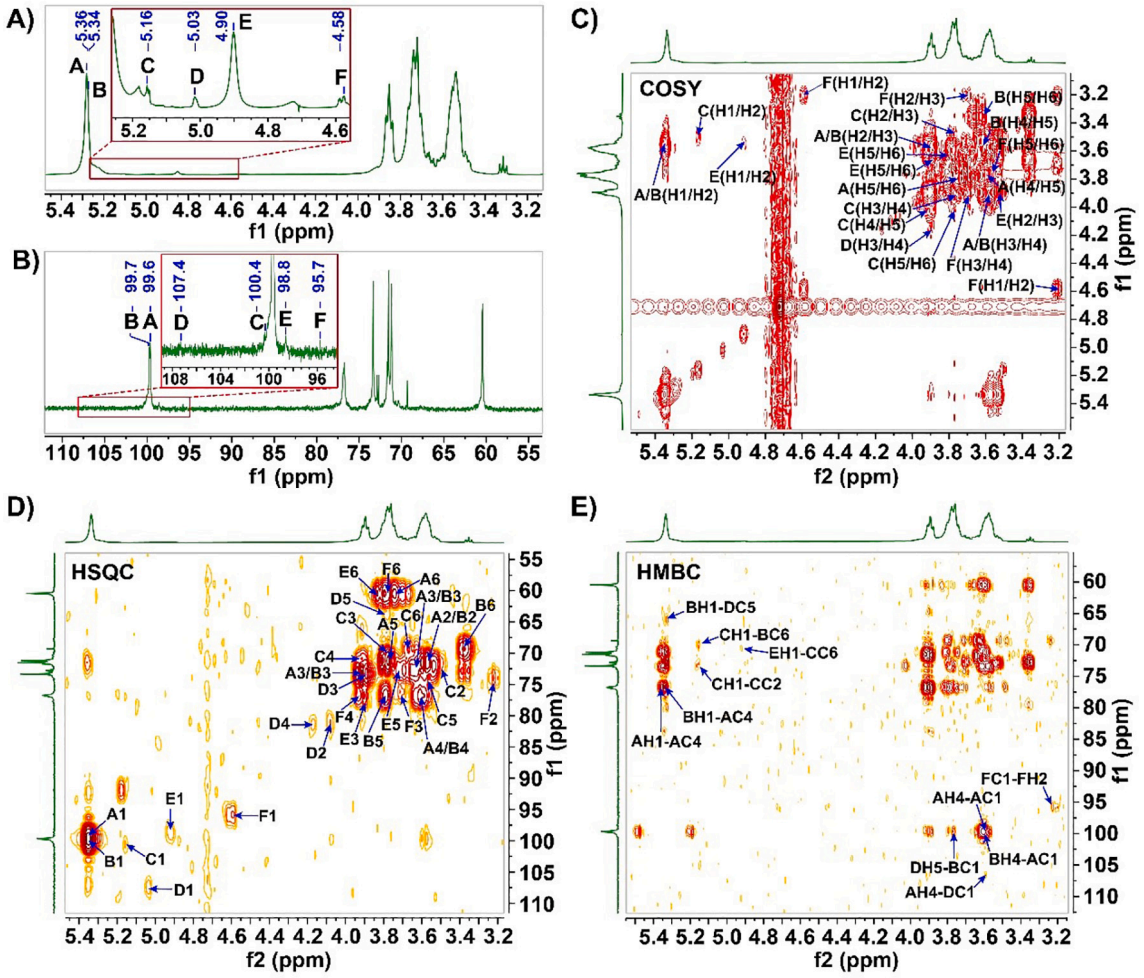

Fig. 4. NMR spectra of APS-B1. (A) ^{1}H NMR spectrum. (B) ^{13}C NMR spectrum. (C) COSY spectrum. (D) HSQC spectrum. (E) HMBC spectrum.

expression levels of p-JNK, p-ERK, and p-p38 were significantly elevated in LPS-induced RAW264.7 macrophages. APS-A1 (200 μg/mL) and APS-B1 (200 μg/mL) treatment dramatically suppressed the phosphorylation of JNK and ERK ($p < 0.05$ or 0.01, *vs.* LPS group) (Fig. 7D–E), but had no significant effect on the phosphorylation of p38 (Fig. 7F).

3.4.5. APS-A1 and APS-B1 inhibited NF-κB activation and P65 nuclear translocation in LPS-induced RAW264.7 macrophages

The NF-κB signal pathway is essential for expressing multiple inflammation-related genes in activated macrophages [40]. The effect of APS-A1 and APS-B1 on the NF-κB signal pathway was investigated. As indicated in Fig. 8A and B, APS-A1 (200 μg/mL) tended to decrease the levels of p-IKK α/β, and APS-B1 (200 μg/mL) markedly reduced the phosphorylation levels of IKK α/β ($p < 0.05$, *vs.* LPS group). In addition, LPS stimulation caused the up-regulation of phosphorylated P65, which was markedly suppressed by both APS-A1 (200 μg/mL) and APS-B1 (200 μg/mL) ($p < 0.05$ or 0.01, *vs.* LPS group) (Fig. 8A and C). NF-κB is sequestered in the cytoplasm by the inhibitory factor IκB α. Hence, the activation of NF-κB also involves the degradation of IκB α [41]. In our study, APS-A1 (200 μg/mL) and APS-B1 (200 μg/mL) treatment prevented LPS-induced degradation of IκB α ($p < 0.05$ or 0.01, *vs.* LPS group) (Fig. 8A and D).

Since nuclear translocation of the NF-κB P65 subunit is a critical step in NF-κB pathway activation, we detected whether APS-A1 and APS-B1 regulated P65 translocation in response to LPS stimulation. As shown in Fig. 8E, P65 translocated from the cytoplasm into the nucleus after LPS stimulation, and APS-A1 (200 μg/mL) and APS-B1 (200 μg/mL) treatment significantly depressed the nuclear translocation of P65. Moreover, western blot analysis also showed that the level of P65 was significantly upregulated in the nucleus and decreased in the cytoplasmic fraction in the LPS group ($p < 0.01$, *vs.* Control group) (Fig. 8F–H). However, APS-A1 (200 μg/mL) and APS-B1 (200 μg/mL) significantly suppressed the translocation of P65 from the cytoplasm to the nucleus ($p < 0.05$ or 0.01, *vs.* LPS group) (Fig. 8F–H). Overall, the inhibitory effect of APS-B1 on NF-κB pathway activation was more pronounced than that of APS-A1.

4. Discussion

The molecular weight, monosaccharide composition, structure of sugar chains, and biological activity of APS in different studies are dissimilar [42]. Polysaccharides in *A. membranaceus* are mainly classified into dextran and heteropolysaccharides [43]. Dextran in *A. membranaceus* were generally identified as α-(1 → 4)-D-glucans. Similar to previous reports, APS-A1 was a homogeneous glucan and comprised of a main chain of 1,4-α-D-Glc*p* with a terminal-α/β-D-Glc*p* attached at the 6-position of every 10 residues (Fig. 5A and C). As for heteropolysaccharides in *A. membranaceus*, its monosaccharide composition is often complex, mainly including glucose, galactose, arabinose, rhamnose, mannose, xylose, fucose, glucuronic acid and galacturonic acid [18,43]. In our study, APS-B1 was a typical heteropolysaccharide. Different from previous research, the backbone of APS-B1 was 1,4-α-D-Glc*p* interspersed with a small amount of 1,5-α-L-Ara*f*, the branches were 1,6-α-D-Gal*p* and terminal-α/β-D-Glc*p* (Fig. 5B and D). The

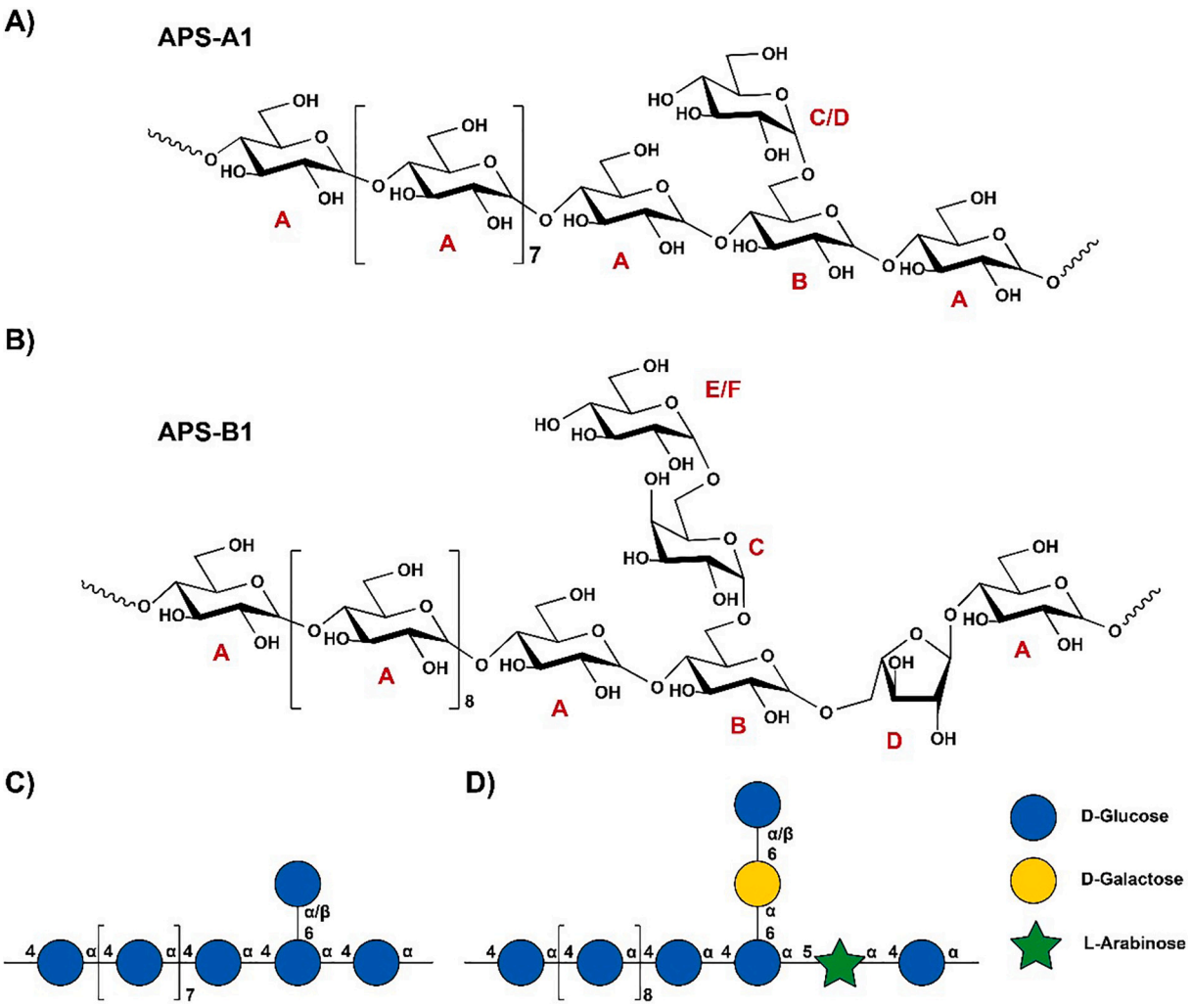

Fig. 5. The predicted chemical structure of APS-A1 and APS-B1. (A) Predicted repeating unit of APS-A1. (B) Predicted repeating unit of APS-B1. (C) Graphical representation of APS-A1. (D) Graphical representation of APS-B1. Graphical symbols are depicted according to the symbol nomenclature for glycans (SNFG).

difference might be due to different origins, growth years, and isolation methods of *A. membranaceus*. APS-A1 and APS-B1 were both large-molecular-weight polysaccharides in *A. membranaceus*, and characterizing their structures would help us further investigate their pharmacological activities.

The chemical structure of polysaccharides is the basis of biological activity. Many factors, including molecular weight, monosaccharide composition, type of glycosidic bonds, and sugar chain conformation, will affect the activity of polysaccharides [44]. In general, polysaccharides with relatively large molecular weight have poor solubility, thus limiting their bioavailability. Meanwhile, too low molecular weight leads to low polymerization and instability of active groups, affecting the biological activity of polysaccharides [45]. For example, two polysaccharides with different molecular weights from *Xylaria nipripes* strains exhibited different anti-inflammatory activity. Notably, the polysaccharide with a larger molecular weight (8.53×10^5 Da) in *Xylaria nipripes* strains displayed more significant anti-inflammatory activity [46]. Similarly, APS-B1 (4.95×10^6 Da), which had a larger molecular weight than APS-A1 (2.62×10^6 Da), also showed more remarkable anti-inflammatory activity in our study (Fig. 8A-H). On the other hand, it has been previously reported that galactose content in polysaccharides is positively correlated with its anti-inflammatory activity in macrophages [47]. Glycosidic bonds →6)-α-D-Gal*p*-(1→ and →5)-α-L-Ara*f*-(1→ were present in the main chain of APS-B1 but not in APS-A1 (Fig. 5A–B), which might be another factor contributing to the difference of anti-inflammatory activity in APS-A1 and APS-B1. In addition, Wang et al. found that the antioxidant capacity of *Phellinus linteus* polysaccharides was positively correlated with their uronic acid content [48]. Liang et al. also confirmed that the higher uronic acid content of black garlic polysaccharides, the stronger their tyrosinase inhibitory, antioxidant, and melanin biosynthesis inhibition activity [49]. In this study, the higher uronic acid content in APS-B1 may also be a reason for its better anti-inflammatory activity. In general, the structural characteristics of polysaccharides were closely related to their specific biological activities. The molecular weight, glycosidic bonds, monosaccharide composition, and uronic acid content may affect their activities.

As critical effector cells of the innate immune system, macrophages have the functions of phagocytosis, secretion, and antigen presentation, which protect the host from external pathogens infection, and invasion [50]. LPS is widely recognized as a potent activator of macrophages and can induce the production of various pro-inflammatory mediators. In this study, we demonstrated that APS-A1 and APS-B1 suppressed the mRNA levels of IL-1β, IL-6, TNF-α, and MCP-1 in LPS-induced RAW264.7 macrophages (Fig. 6C–F). Among them, IL-1β , a cardinal cytokine of innate immunity, can stimulate the production of other inflammatory cytokines, including TNF-α and IL-6, which are directly or indirectly involved in many illnesses [51]. TNF-α participates in normal inflammatory responses, promotes tissue repair, and induces tumor cell apoptosis. And IL-6 is a multifunctional cytokine that regulates the

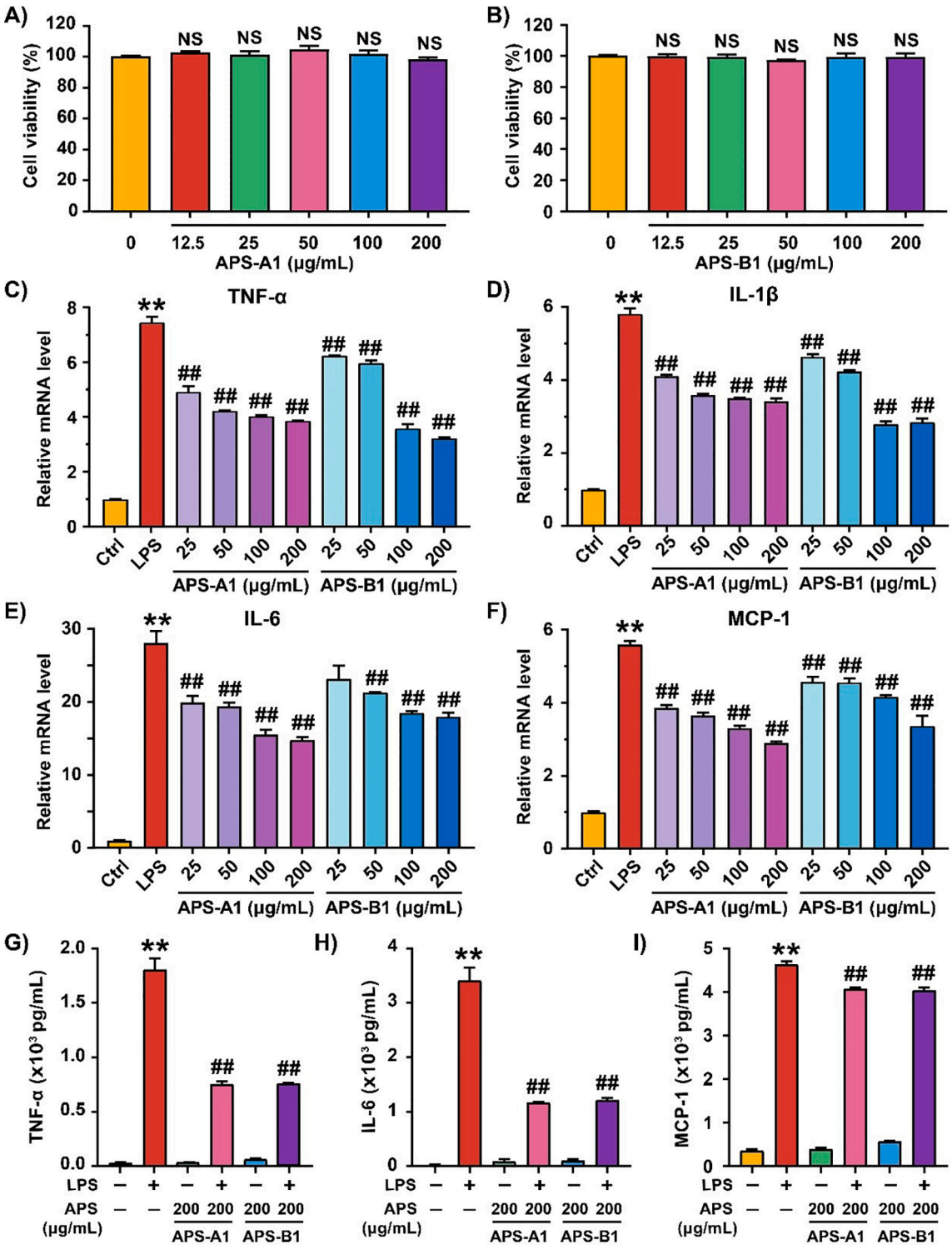

Fig. 6. Cytotoxic and anti-inflammatory activities of APS-A1 and APS-B1 on RAW264.7 macrophages. (A–B) Effect of APS-A1 (A) and APS-B1 (B) on viability of RAW264.7 macrophages. (C-F) Suppressive effect of APS-A1 and APS-B1 on mRNA levels of TNF-α (C), IL-1β (D), IL-6 (E), and MCP-1 (F) in LPS-induced RAW264.7 macrophages. (G–I) Inhibitory effect of APS-A1 and APS-B1 on production of TNF-α (G), IL-6 (H), and MCP-1 (I) induced in LPS-induced RAW264.7 macrophages. Data were presented as means ± SD ($n = 3$). ** $p < 0.01$ *vs.* Control group; # $p < 0.05$, ## $p < 0.01$ *vs.* LPS group.

growth and differentiation of many cells [52]. TNF-α, IL-1β, and IL-6 are crucial inflammatory cytokines that can be involved in inflammatory responses in various pathways, thus inducing an inflammatory cascade [53]. MCP-1 is a monocyte chemokine that participates in inflammation responses by recruiting monocytes [54]. In addition, APS-A1 and APS-B1 also reduced the expression of classical pro-inflammatory proteins (NLRP3, iNOS, and COX-2) (Fig. 7A–C), thereby inhibiting the massive secretion of inflammatory mediators and pro-inflammatory cytokines. The above results all confirmed that APS-A1 and APS-B1 had potential anti-inflammatory activities.

Although the signal pathways involved in inflammation are diverse and complex, MAPK and NF-κB signaling pathways have been

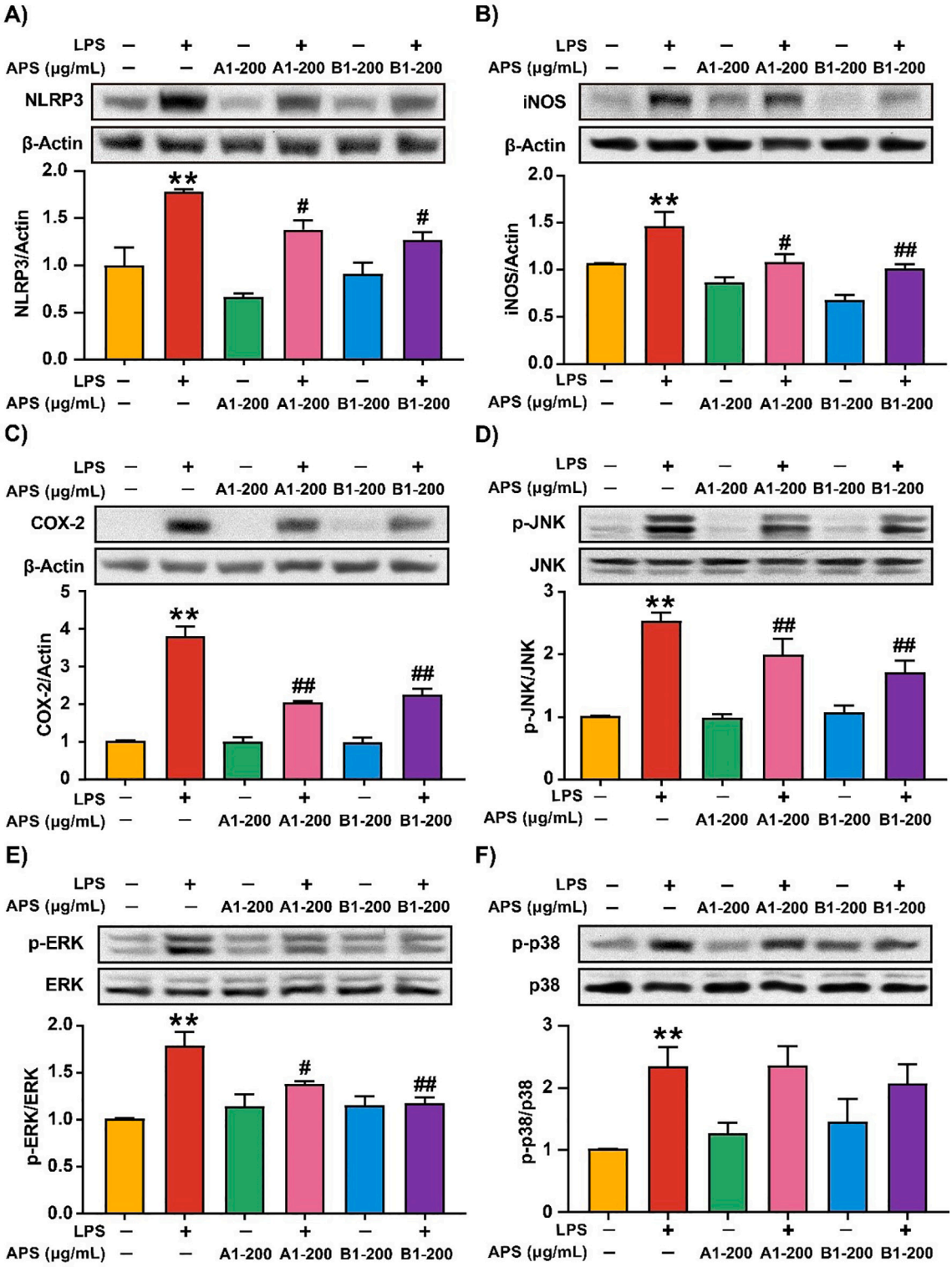

Fig. 7. Suppressive effect of APS-A1 and APS-B1 on expressions of NLRP3, iNOS, COX-2, and MAPK signal pathway in LPS-induced RAW264.7 macrophages. Cells were pre-treated with APS-A1 and APS-B1 for 12 h, followed by LPS (1 μg/mL) stimulation for 24 h. Then the protein levels of NLRP3 (A), COX-2 (B), and iNOS (C) and the phosphorylated levels of JNK (D), ERK (E), and p38 (F) were determined by Western blot analysis, and their relative change was quantified. Data were presented as means ± SD ($n = 3$). $^{**}p < 0.01$ *vs.* Control group; $^{\#}p < 0.05$, $^{\#\#}p < 0.01$ *vs.* LPS group.

considered the core pathways regulating inflammatory mediators and cytokines [55]. LPS-stimulation activates phosphorylation of MAPK family members JNK, ERK, and p38 in RAW264.7 macrophages, thereby mediating a variety of inflammatory reactions, such as the production of proinflammatory mediators, and the migration and apoptosis of macrophages [56]. In our research, we found that APS-A1 and APS-B1 treatment inhibited the phosphorylation of JNK and ERK, but not p38 (Fig. 7D–F), which indicated that the inhibition of MAPK signaling pathway by APS-A1 and APS-B1 was selective. Previous studies have demonstrated that *Smilax china* L. polysaccharides and *Ganoderma*

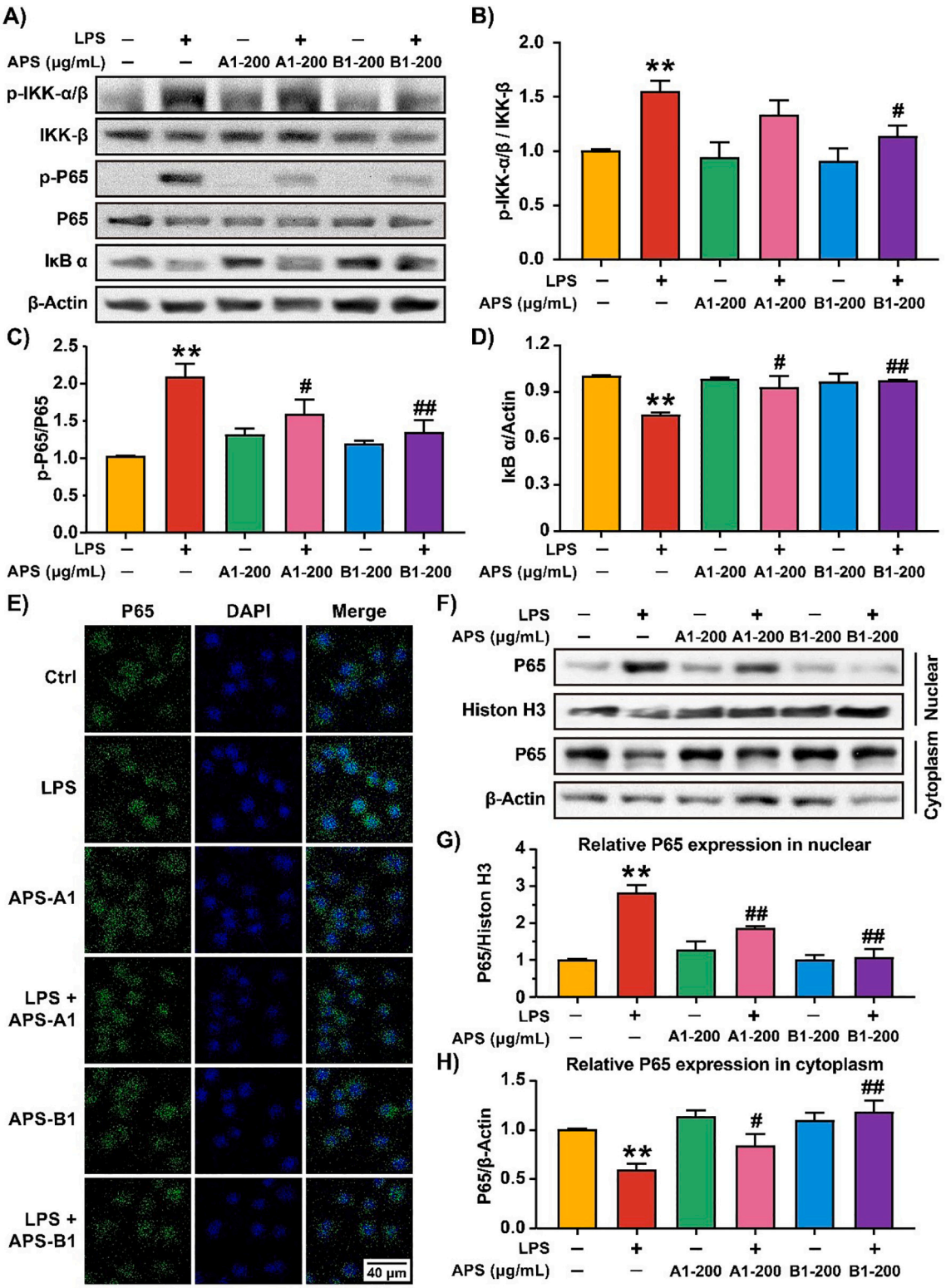

Fig. 8. Effects of APS-A1 and APS-B1 on LPS-induced NF-κB signal pathway in RAW264.7 cells. (A–D) The protein levels of p-p65, p65, IκB α, p-IKK α/β, and IKK-β were determined by Western blot analysis, and the relative change was quantified. (E) Cells were pre-treated with APS-A1 (200 μg/ mL) and APS-B1 (200 μg/ mL) for 12 h and then exposed to LPS (1 μg/mL) for 1 h. Then, the localization of NF-κB was analyzed by double immunofluorescent staining of the NF-κB P65 subunit (green) and nucleus (blue). (F-H) The nuclear and cytoplasmic fractions of cells were separated using a nuclear and cytoplasmic protein extraction kit. The protein level of p65 in cytoplasmic and nuclear fractions was determined by western blot analysis, and the relative change was quantified. Data were presented as means ± SD (n = 3). ** $p < 0.01$ *vs.* Control group; # $p < 0.05$, ## $p < 0.01$ *vs.* LPS group. (For interpretation of the references to colour in this figure legend, the reader is referred to the web version of this article.)

lucidum polysaccharides could inhibit phosphorylation of ERK and JNK [57,58], while Plumula Nelumbinis polysaccharides inhibit phosphorylation of p38, JNK, and ERK [59]. Different polysaccharides activate different MAPK pathway sites, which may be attributed by the structural differences of polysaccharides.

NF-κB is an essential transcription factor complex involved in the regulation of many inflammatory factors. Under physiological conditions, NF-κB exists in the cytoplasm in an inactive form and combines with its inhibitor IκB α to form a complex. In contrast, when the inflammatory reaction occurs, the IKK protein phosphorylates and activates the ubiquitin-proteasome pathway to degrade IκB α. Then free NF-κB P65 transposed into the nucleus, inducing the expression of multiple inflammatory genes [60]. In our study, APS-A1 and APS-B1 treatment not only inhibited the phosphorylation of IKK (Fig. 8A–C) and blocked the degradation of IκB α (Fig. 8D), but also inhibited the nuclear translocation of P65 (Fig. 8E–H). It is worth mentioning that the anti-inflammatory effect may come from the particularity of the structure. Many studies have demonstrated that APS with α-(1, 4)-glucose as backbone were ligands of TLR4 and could competitively inhibit the specific binding of LPS to macrophages [61,62]. Specifically, APS-A1 and APS-B1 with α-(1 → 4)-D-glucans structure might competitively inhibit the binding of LPS to TLR4 and thus suppress LPS-induced inflammatory responses by NF-κB and MAPK (ERK, JNK) signal pathways. Similarly, a polysaccharide of marine filamentous fungus with a structural backbone similar to APS-A1 and APS-B1, could inhibit the stimulation of LPS on macrophages [63]. The relationship between the anti-inflammatory mechanism and structure of APS-A1 and APS-B1 still requires further study.

5. Conclusions

This study isolated two novel polysaccharides (APS-A1 and APS-B1) with molecular weights of 2.62×10^6 Da and 4.95×10^6 Da from *A. membranaceus*. Structural analysis showed that APS-A1 was a 1,4-α-D-Glc*p* backbone with a 1,4,6-α-D-Glc*p* branch every ten residues. The backbone of APS-B1 consisted of 1,4-α-D-Glc*p*, 1,4,6-α-D-Glc*p*, 1,5-α-L-Ara*f* and the sidechains composed of 1,6-α-D-Gal*p* and T-α/β-Glc*p*. Further, both APS-A1 and APS-B1 performed anti-inflammatory activities *in vitro*. They reduced the production of TNF-α, IL-6, and MCP-1 *via* suppression of NF-κB and MAPK (ERK, JNK) signal pathways in LPS-induced RAW264.7 macrophages. Altogether, the results suggested that APS-A1 and APS-B1 could be potential anti-inflammatory supplements. Further studies will focus on their bioactivity and structure-activity relationship.

CRediT authorship contribution statement

Guangming Chen: Conceptualization, Methodology, Validation, Writing – original draft, Writing – review & editing. **Nan Jiang:** Investigation, Resources. **Junping Zheng:** Data curation. **Haiming Hu:** Methodology, Investigation. **Huabing Yang:** Methodology, Supervision. **Aizhen Lin:** Investigation, Resources. **Baifei Hu:** Conceptualization, Methodology, Investigation, Validation, Writing – review & editing. **Hongtao Liu:** Conceptualization, Resources, Writing – review & editing, Project administration, Funding acquisition.

Declaration of competing interest

The authors declare that there is no conflict of interest.

Data availability

Data will be made available on request.

Acknowledgments

This work was supported by Department of Science and Technology of Hubei Province [grant number 2021CFA014]; Major Science and Technology Project in Yunnan Province [grant number 202102AE090042], Knowledge Innovation Program of Wuhan [grant number 2022020801010420], and Health Commission of Hubei Province of China [grant number ZY2021Z005].

Appendix A. Supplementary data

Supplementary data to this article can be found online at https://doi.org/10.1016/j.ijbiomac.2023.124386.

References

[1] R. Medzhitov, Origin and physiological roles of inflammation, Nature 454 (7203) (2008) 428–435, https://doi.org/10.1038/nature07201.
[2] E. Oikonomou, M. Leopoulou, P. Theofilis, A.S. Antonopoulos, G. Siasos, G. Latsios, V.C. Mystakidi, C. Antoniades, D. Tousoulis, A link between inflammation and thrombosis in atherosclerotic cardiovascular diseases: clinical and therapeutic implications, Atherosclerosis 309 (2020) 16–26, https://doi.org/10.1016/j.atherosclerosis.2020.07.027.
[3] M. Liu, W. Li, Y. Chen, X. Wan, J. Wang, Fucoxanthin: a promising compound for human inflammation-related diseases, Life Sci. 255 (2020), 117850, https://doi.org/10.1016/j.lfs.2020.117850.
[4] P. Roth, W. Wick, M. Weller, Steroids in neurooncology: actions, indications, side-effects, Curr. Opin. Neurol. 23 (6) (2010) 597–602, https://doi.org/10.1097/WCO.0b013e32833e5a5d.
[5] N. El Menyiy, A. El Allam, S. Aboulaghras, I. Jaouadi, S. Bakrim, N. El Omari, M. A. Shariati, A. Miftakhutdinov, P. Wilairatana, M.S. Mubarak, A. Bouyahya, Inflammatory auto-immune diseases of the intestine and their management by natural bioactive compounds, Biomed. Pharmacother. 151 (2022), 113158, https://doi.org/10.1016/j.biopha.2022.113158.
[6] C. Hou, L. Chen, L. Yang, X. Ji, An insight into anti-inflammatory effects of natural polysaccharides, Int. J. Biol. Macromol. 153 (2020) 248–255, https://doi.org/10.1016/j.ijbiomac.2020.02.315.
[7] Y. Yu, M. Shen, Q. Song, J. Xie, Biological activities and pharmaceutical applications of polysaccharide from natural resources: a review, Carbohydr. Polym. 183 (2018) 91–101, https://doi.org/10.1016/j.carbpol.2017.12.009.
[8] Y. Yang, Z. Qiu, L. Li, S.K. Vidyarthi, Z. Zheng, R. Zhang, Structural characterization and antioxidant activities of one neutral polysaccharide and three acid polysaccharides from Ziziphus jujuba cv. Hamidazao: a comparison, Carbohydr. Polym. 261 (2021), 117879, https://doi.org/10.1016/j.carbpol.2021.117879.
[9] J.Y. Yin, B.C. Chan, H. Yu, I.Y. Lau, X.Q. Han, S.W. Cheng, C.K. Wong, C.B. Lau, M. Y. Xie, K.P. Fung, P.C. Leung, Q.B. Han, Separation, structure characterization, conformation and immunomodulating effect of a hyperbranched heteroglycan from Radix Astragali, Carbohydr. Polym. 87 (1) (2012) 667–675, https://doi.org/10.1016/j.carbpol.2011.08.045.
[10] X.Y. Wang, D.D. Zhang, J.Y. Yin, S.P. Nie, M.Y. Xie, Recent developments in Hericium erinaceus polysaccharides: extraction, purification, structural characteristics and biological activities, Crit. Rev. Food Sci. Nutr. 59 (sup1) (2019) S96–S115, https://doi.org/10.1080/10408398.2018.1521370.
[11] C.H. Zhang, X. Yang, J.R. Wei, N.M. Chen, J.P. Xu, Y.Q. Bi, M. Yang, X. Gong, Z. Y. Li, K. Ren, Q.H. Han, L. Zhang, X. Li, M.Y. Ji, C.C. Wang, M.H. Li, Ethnopharmacology, phytochemistry, pharmacology, toxicology and clinical applications of Radix Astragali, Chin. J. Integr. Med. 27 (3) (2021) 229–240, https://doi.org/10.1007/s11655-019-3032-8.
[12] Z. Chen, L. Liu, C. Gao, W. Chen, C.T. Vong, P. Yao, Y. Yang, X. Li, X. Tang, S. Wang, Y. Wang, Astragali Radix (Huangqi): a promising edible immunomodulatory herbal medicine, J. Ethnopharmacol. 258 (2020), 112895, https://doi.org/10.1016/j.jep.2020.112895.
[13] Y. Yin, H. Li, Y. Chen, R. Zhu, L. Li, X. Zhang, J. Zhou, Z. Wang, X. Li, Combination of Astragalus membranaceus and Angelica sinensis ameliorates vascular endothelial cell dysfunction by inhibiting oxidative stress, Evid. Based Complement. Alternat. Med. 2020 (2020) 6031782, https://doi.org/10.1155/2020/6031782.
[14] P.K. Lai, J.Y. Chan, S.B. Wu, L. Cheng, G.K. Ho, C.P. Lau, E.J. Kennelly, P.C. Leung, K.P. Fung, C.B. Lau, Anti-inflammatory activities of an active fraction isolated from the root of Astragalus membranaceus in RAW 264.7 macrophages, Phytother. Res. 28 (3) (2014) 395–404, https://doi.org/10.1002/ptr.5002.
[15] Y. Liang, Q. Zhang, L. Zhang, R. Wang, X. Xu, X. Hu, Astragalus membranaceus treatment protects Raw264.7 cells from influenza virus by regulating G1 phase and the TLR3-mediated signaling pathway, Evid. Based Complement. Alternat. Med. 2019 (2019), 2971604, https://doi.org/10.1155/2019/2971604.
[16] J.Y. Chan, F.C. Lam, P.C. Leung, C.T. Che, K.P. Fung, Antihyperglycemic and antioxidative effects of a herbal formulation of Radix Astragali, Radix Codonopsis and Cortex Lycii in a mouse model of type 2 diabetes mellitus, Phytother. Res. 23 (5) (2009) 658–665, https://doi.org/10.1002/ptr.2694.

[17] B. Salehi, J.N.P. Carneiro, J.E. Rocha, H.D.M. Coutinho, M.F.B.Morais Braga, J. Sharifi-Rad, P. Semwal, S. Painuli, L.M. Moujir, V. de Zarate Machado, S. Janakiram, N.V.Anil Kumar, M. Martorell, N. Cruz-Martins, M.El Beyrouthy, C. Sadaka, Astragalus species: insights on its chemical composition toward pharmacological applications, Phytother. Res. (2020), https://doi.org/10.1002/ptr.6974.

[18] J. Fu, Z. Wang, L. Huang, S. Zheng, D. Wang, S. Chen, H. Zhang, S. Yang, Review of the botanical characteristics, phytochemistry, and pharmacology of Astragalus membranaceus (Huangqi), Phytother. Res. 28 (9) (2014) 1275–1283, https://doi.org/10.1002/ptr.5188.

[19] P. Yi, N. Li, J.B. Wan, D. Zhang, M. Li, C. Yan, Structural characterization and antioxidant activity of a heteropolysaccharide from Ganoderma capense, Carbohydr. Polym. 121 (2015) 183–189, https://doi.org/10.1016/j.carbpol.2014.11.034.

[20] M. DuBois, K.A. Gilles, J.K. Hamilton, P.A. Rebers, F. Smith, Colorimetric method for determination of sugars and related substances, Anal. Chem. 28 (1956) 350–356, https://doi.org/10.1021/ac60111a017.

[21] L.S. McKee, Measuring enzyme kinetics of glycoside hydrolases using the 3,5-dinitrosalicylic acid assay, Methods Mol. Biol. 1588 (2017) 27–36, https://doi.org/10.1007/978-1-4939-6899-2_3.

[22] M.M. Bradford, A rapid and sensitive method for the quantitation of microgram quantities of protein utilizing the principle of protein-dye binding, Anal. Biochem. 72 (1976) 248–254, https://doi.org/10.1016/0003-2697(76)90527-3.

[23] P. Kumar, V. Kumar, Estimation of uronic acids using diverse approaches and monosaccharide composition of alkali soluble polysaccharide from Vitex negundo Linn, Carbohydr. Polym. 165 (2017) 205–212, https://doi.org/10.1016/j.carbpol.2017.02.034.

[24] L. Zhu, G. Chen, Y. Guo, J. Zheng, H. Yang, X. Sun, Y. Liu, B. Hu, H. Liu, Structural characterization of Poria cocos oligosaccharides and their effects on the hepatic metabolome in high-fat diet-fed mice, Food Funct. 13 (12) (2022) 6813–6829, https://doi.org/10.1039/d2fo00638c.

[25] S. Hakomori, A rapid permethylation of glycolipid, and polysaccharide catalyzed by methylsulfinyl carbanion in dimethyl sulfoxide, J.Biochem. 55 (1964) 205–208, https://doi.org/10.1093/oxfordjournals.jbchem.a127869.

[26] J. Zheng, G. Cheng, Q. Li, S. Jiao, C. Feng, X. Zhao, H. Yin, Y. Du, H. Liu, Chitin oligosaccharide modulates gut microbiota and attenuates high-fat-diet-induced metabolic syndrome in mice, Mar. Drugs 16 (2) (2018), https://doi.org/10.3390/md16020066.

[27] J.H. Wang, J.L. Xu, J.C. Zhang, Y. Liu, H.J. Sun, X. Zha, Physicochemical properties and antioxidant activities of polysaccharide from floral mushroom cultivated in Huangshan Mountain, Carbohydr. Polym. 131 (2015) 240–247, https://doi.org/10.1016/j.carbpol.2015.05.052.

[28] W. Chen, X. Zhu, J. Ma, M. Zhang, H. Wu, Structural elucidation of a novel pectin-polysaccharide from the petal of Saussurea laniceps and the mechanism of its anti-HBV activity, Carbohydr. Polym. 223 (2019), 115077, https://doi.org/10.1016/j.carbpol.2019.115077.

[29] X.Q. Zha, C.Q. Lu, S.H. Cui, L.H. Pan, H.L. Zhang, J.H. Wang, J.P. Luo, Structural identification and immunostimulating activity of a Laminaria japonica polysaccharide, Int. J. Biol. Macromol. 78 (2015) 429–438, https://doi.org/10.1016/j.ijbiomac.2015.04.047.

[30] X. Ji, Y. Yan, C. Hou, M. Shi, Y. Liu, Structural characterization of a galacturonic acid-rich polysaccharide from Ziziphus jujuba cv.Muzao, Int. J. Biol. Macromol. 147 (2020) 844–852, https://doi.org/10.1016/j.ijbiomac.2019.09.244.

[31] Y. Cheng, Y. Xie, J.C. Ge, L. Wang, D.Y. Peng, N.J. Yu, Y. Zhang, Y.H. Jiang, J. P. Luo, W.D. Chen, Structural characterization and hepatoprotective activity of a galactoglucan from Poria cocos, Carbohydr. Polym. 263 (2021), 117979, https://doi.org/10.1016/j.carbpol.2021.117979.

[32] Y. Su, H. Li, Z. Hu, Y. Zhang, L. Guo, M. Shao, C. Man, Y. Jiang, Research on degradation of polysaccharides during Hericium erinaceus fermentation, LWT 173 (2023), https://doi.org/10.1016/j.lwt.2022.114276.

[33] H.B. Hu, H.P. Liang, H.M. Li, R.N. Yuan, J. Sun, L.L. Zhang, M.H. Han, Y. Wu, Isolation, purification, characterization and antioxidant activity of polysaccharides from the stem barks of Acanthopanax leucorrhizus, Carbohydr. Polym. 196 (2018) 359–367, https://doi.org/10.1016/j.carbpol.2018.05.028.

[34] Z. Zhang, L. Guo, A. Yan, L. Feng, Y. Wan, Fractionation, structure and conformation characterization of polysaccharides from Anoectochilus roxburghii, Carbohydr. Polym. 231 (2020), 115688, https://doi.org/10.1016/j.carbpol.2019.115688.

[35] P. Mutaillifu, K. Bobakulov, A. Abuduwaili, H. Huojiaaihemaiti, R. Nuerxiati, H. A. Aisa, A. Yili, Structural characterization and antioxidant activities of a water soluble polysaccharide isolated from Glycyrrhiza glabra, Int. J. Biol. Macromol. 144 (2020) 751–759, https://doi.org/10.1016/j.ijbiomac.2019.11.245.

[36] Y. Liu, Y. Ye, X. Hu, J. Wang, Structural characterization and anti-inflammatory activity of a polysaccharide from the lignified okra, Carbohydr. Polym. 265 (2021), 118081, https://doi.org/10.1016/j.carbpol.2021.118081.

[37] Z. Sheng, J. Liu, B. Yang, Structure differences of water soluble polysaccharides in Astragalus membranaceus induced by origin and their bioactivity, Foods 10 (8) (2021), https://doi.org/10.3390/foods10081755.

[38] C.C. Su, S.C. Wang, I.C. Chen, F.Y. Chiu, P.L. Liu, C.H. Huang, K.H. Huang, S. H. Fang, W.C. Cheng, S.P. Huang, H.C. Yeh, C.C. Liu, P.Y. Lee, M.Y. Huang, C.Y. Li, Zerumbone suppresses the LPS-induced inflammatory response and represses activation of the NLRP3 inflammasome in macrophages, Front. Pharmacol. 12 (2021), 652860, https://doi.org/10.3389/fphar.2021.652860.

[39] W. Rod-In, C. Monmai, I.S. Shin, S. You, W.J. Park, Neutral lipids, glycolipids, and phospholipids, isolated from sandfish (Arctoscopus japonicus) eggs, exhibit anti-inflammatory activity in LPS-stimulated RAW264.7 cells through NF-kappaB and MAPKs pathways, Mar. Drugs 18 (9) (2020), https://doi.org/10.3390/md18090480.

[40] T. Lawrence, The nuclear factor NF-kappaB pathway in inflammation, Cold Spring Harb. Perspect. Biol. 1 (6) (2009), a001651, https://doi.org/10.1101/cshperspect.a001651.

[41] T. Henkel, T. Machleidt, I. Alkalay, M. Kronke, Y. Ben-Neriah, P.A. Baeuerle, Rapid proteolysis of I kappa B-alpha is necessary for activation of transcription factor NF-kappa B, Nature 365 (6442) (1993) 182–185.

[42] Y. Du, H. Wan, P. Huang, J. Yang, Y. He, A critical review of Astragalus polysaccharides: from therapeutic mechanisms to pharmaceutics, Biomed. Pharmacother. 147 (2022), 112654, https://doi.org/10.1016/j.biopha.2022.112654.

[43] M. Jin, K. Zhao, Q. Huang, P. Shang, Structural features and biological activities of the polysaccharides from Astragalus membranaceus, Int. J. Biol. Macromol. 64 (2014) 257–266, https://doi.org/10.1016/j.ijbiomac.2013.12.002.

[44] Y. Yi, W. Xu, H.X. Wang, F. Huang, L.M. Wang, Natural polysaccharides experience physiochemical and functional changes during preparation: a review, Carbohydr. Polym. 234 (2020), 115896, https://doi.org/10.1016/j.carbpol.2020.115896.

[45] J.H. Xie, M.L. Jin, G.A. Morris, X.Q. Zha, H.Q. Chen, Y. Yi, J.E. Li, Z.J. Wang, J. Gao, S.P. Nie, P. Shang, M.Y. Xie, Advances on bioactive polysaccharides from medicinal plants, Crit. Rev. Food Sci. Nutr. 56 (Suppl 1) (2016) S60–S84, https://doi.org/10.1080/10408398.2015.1069255.

[46] C.F. Chen, C.H. Su, M.N. Lai, L.T. Ng, Differences in water soluble non-digestible polysaccharides and anti-inflammatory activities of fruiting bodies from two cultivated Xylaria nigripes strains, Int. J. Biol. Macromol. 116 (2018) 728–734, https://doi.org/10.1016/j.ijbiomac.2018.05.047.

[47] M.-K. Lu, J.-J. Cheng, C.-Y. Lin, C.-C. Chang, Purification, structural elucidation, and anti-inflammatory effect of a water-soluble 1,6-branched 1,3-α-d-galactan from cultured mycelia of Poria cocos, Food Chem. 118 (2) (2010) 349–356, https://doi.org/10.1016/j.foodchem.2009.04.126.

[48] Z.B. Wang, J.J. Pei, H.L. Ma, P.F. Cai, J.K. Yan, Effect of extraction media on preliminary characterizations and antioxidant activities of Phellinus linteus polysaccharides, Carbohydr. Polym. 109 (2014) 49–55, https://doi.org/10.1016/j.carbpol.2014.03.057.

[49] J. Liang, Y. Zhao, F. Yang, L. Zheng, Y. Ma, Q. Liu, L. Cai, W. Gong, B. Wang, Preparation and structure-activity relationship of highly active black garlic polysaccharides, Int. J. Biol. Macromol. 220 (2022) 601–612, https://doi.org/10.1016/j.ijbiomac.2022.08.115.

[50] J.M. Ehrchen, J. Roth, K. Barczyk-Kahlert, More than suppression: glucocorticoid action on monocytes and macrophages, Front. Immunol. 10 (2019) 2028, https://doi.org/10.3389/fimmu.2019.02028.

[51] C.A. Dinarello, Interleukin-1 in the pathogenesis and treatment of inflammatory diseases, Blood 117 (14) (2011) 3720–3732, https://doi.org/10.1182/blood-2010-07-273417.

[52] M. Kapoor, J. Martel-Pelletier, D. Lajeunesse, J.P. Pelletier, H. Fahmi, Role of proinflammatory cytokines in the pathophysiology of osteoarthritis, Nat. Rev. Rheumatol. 7 (1) (2011) 33–42, https://doi.org/10.1038/nrrheum.2010.196.

[53] L. Ni, L. Wang, X. Fu, D. Duan, Y.J. Jeon, J. Xu, X. Gao, In vitro and in vivo anti-inflammatory activities of a fucose-rich fucoidan isolated from Saccharina japonica, Int. J. Biol. Macromol. 156 (2020) 717–729, https://doi.org/10.1016/j.ijbiomac.2020.04.012.

[54] V. Bianconi, A. Sahebkar, S.L. Atkin, M. Pirro, The regulation and importance of monocyte chemoattractant protein-1, Curr. Opin. Hematol. 25 (1) (2018) 44–51, https://doi.org/10.1097/MOH.0000000000000389.

[55] Y. Fang, L. Yang, J. He, Plantanone C attenuates LPS-stimulated inflammation by inhibiting NF-kappaB/iNOS/COX-2/MAPKs/Akt pathways in RAW 264.7 macrophages, Biomed. Pharmacother. 143 (2021), 112104, https://doi.org/10.1016/j.biopha.2021.112104.

[56] C. Xie, M. Ge, J. Jin, H. Xu, L. Mao, S. Geng, J. Wu, J. Zhu, X. Li, C. Zhong, Mechanism investigation on bisphenol S-induced oxidative stress and inflammation in murine RAW264.7 cells: the role of NLRP3 inflammasome, TLR4, Nrf2 and MAPK, J. Hazard. Mater. 394 (2020), 122549, https://doi.org/10.1016/j.jhazmat.2020.122549.

[57] Y. Zhang, X. Pan, S. Ran, K. Wang, Purification, structural elucidation and anti-inflammatory activity in vitro of polysaccharides from Smilax china L, Int. J. Biol. Macromol. 139 (2019) 233–243, https://doi.org/10.1016/j.ijbiomac.2019.07.209.

[58] C. Guo, D. Guo, L. Fang, T. Sang, J. Wu, C. Guo, Y. Wang, Y. Wang, C. Chen, J. Chen, R. Chen, X. Wang, Ganoderma lucidum polysaccharide modulates gut microbiota and immune cell function to inhibit inflammation and tumorigenesis in colon, Carbohydr. Polym. 267 (2021), 118231, https://doi.org/10.1016/j.carbpol.2021.118231.

[59] Q. Zheng, J. Chen, Y. Yuan, X. Zhang, L. Li, Y. Zhai, X. Gong, B. Li, Structural characterization, antioxidant, and anti-inflammatory activity of polysaccharides from Plumula nelumbinis, Int. J. Biol. Macromol. 212 (2022) 111–122, https://doi.org/10.1016/j.ijbiomac.2022.05.097.

[60] J. Qiao, L.H. Xu, J. He, D.Y. Ouyang, X.H. He, Cucurbitacin E exhibits anti-inflammatory effect in RAW 264.7 cells via suppression of NF-kappaB nuclear translocation, Inflamm. Res. 62 (5) (2013) 461–469, https://doi.org/10.1007/s00011-013-0598-z.

[61] X. Zhang, C. Qi, Y. Guo, W. Zhou, Y. Zhang, Toll-like receptor 4-related immunostimulatory polysaccharides: primary structure, activity relationships, and

possible interaction models, Carbohydr. Polym. 149 (2016) 186–206, https://doi.org/10.1016/j.carbpol.2016.04.097.

[62] W. Wei, H.T. Xiao, W.R. Bao, D.L. Ma, C.H. Leung, X.Q. Han, C.H. Ko, C.B. Lau, C. K. Wong, K.P. Fung, P.C. Leung, Z.X. Bian, Q.B. Han, TLR-4 may mediate signaling pathways of Astragalus polysaccharide RAP induced cytokine expression of RAW264.7 cells, J. Ethnopharmacol. 179 (2016) 243–252, https://doi.org/10.1016/j.jep.2015.12.060.

[63] S. Chen, D.K. Yin, W.B. Yao, Y.D. Wang, Y.R. Zhang, X.D. Gao, Macrophage receptors of polysaccharide isolated from a marine filamentous fungus Phoma herbarum YS4108, Acta Pharmacol. Sin. 30 (7) (2009) 1008–1014, https://doi.org/10.1038/aps.2009.93.